Draft version February 4, 2025
Typeset using LaTeX **twocolumn** style in AASTeX631

# Gravitational Lensing: Mechanism of formation of SN 2022 QMX

Yixuan Shao[1]

[1]*Department of Physics and Astronomy, Stony Brook University, Stony Brook, NY 11794, USA*

## ABSTRACT

The phenomenon of gravitational lensing, as predicted by Einstein's theory of general relativity, provides a unique window into the understanding of the universe's structure and the distribution of dark matter. The Einstein Cross configuration observed in SN 2022 QMX (Goobar et al. (2023)) offers a rare and significant opportunity to study these effects in unprecedented detail. This paper will focus on the theoretical background of the Einstein Cross phenomenon, with a particular emphasis on the role of quadrupole distortion in the gravitational lensing effect. By applying the theory of quadrupole distortion, we analyze the light paths bent by the gravitational field of an intervening galaxy, leading to the formation of the characteristic cross-shaped image as seen in the case of SN 2022 QMX. The results highlight the significance of quadrupole distortion in enhancing our understanding of the mass distribution within the lensing galaxy and offer insights into the potential for using similar events to probe dark matter and the expansion rate of the universe.

## 1. INTRODUCTION

"SN Zwicky" (a.k.a. ZTF22aaylnhq and SN 2022 qmx), a Supernovae Ia with redshift $z = 0.35$ (which we could essentially negligible sensitivity for detection in Bright Transient Survey(BTS)) and located at right ascension $17^h35^m44.32^s$ and declination $4°49'59.60''$ (J2000), was detected by Zwicky Transient Facility (ZTF) on August 2022 (Goobar et al. (2022)).

Type Ia supernovae, such as SN Zwicky, serve as critical tools for understanding the universe. They are used as standard candles in cosmology due to their consistent peak luminosity, allowing astronomers to measure cosmic distances and study the expansion of the universe. However, the observation of SN Zwicky offers more than just a measure of distance; it provides a unique opportunity and view to explore the intricate phenomena of gravitational lensing and quadrupole distortion.

In the first part we will generally introduce Gravitational lensing which is a prediction of Einstein's theory of General Relativity (GR), occurs when the gravitational field of a massive object (such as a galaxy of a cluster of galaxies) warps the fabric of spacetime, bending the path of light traveling near it. This effect can magnify and distort the images of distant astronomical objects, such as supernovae, allowing us to observe them in greater detail than would otherwise be possible. And this method makes possible our observations of even more distant astronomical objects.

Furthermore, light is an electromagnetic wave, which means that by introducing quadrupole distortion borrowed from electromagnetic wave theory we can better explain the mechanism of the image characteristics of Einstein's cross and the principle behind it. Quadrupole distortion also provides a framework for understanding the asymmetries in the gravitational field of the lensing mass. Through the approach of Turyshev & Toth (2021a), we can investigate the direct relationship between the algebraic characteristics of the quartic solution for the electromagnetic (EM) field, the astroid caustic geometric properties, and the resulting Einstein cross's geometry and shape as observed on the image plane of a thin lens telescope. By studying the quadrupole distortion evident in the lensing of SN Zwicky, researchers can gain insights into the complex mass distribution within the lensing galaxy or cluster, offering clues to the underlying structure of cosmic matter.

This study seeks to explore the theoretical foundations of gravitational lensing and quadrupole distortion, applying these principles to the observation of SN Zwicky. Through a combination of theoretical analysis and observations, we seek to enhance our understanding of the universe's structure, the distribution of dark matter, and the principles governing the bending of light in the cosmos.

## 2. GRAVITATIONAL LENS

A lesser-known yet significant detail predates the formalization of general relativity: In 1912, a full three years before his monumental breakthrough, Einstein succinctly described one of the pivotal outcomes of light

deflection—the potential for a geometric gravitational lens. (Sauer (2010))

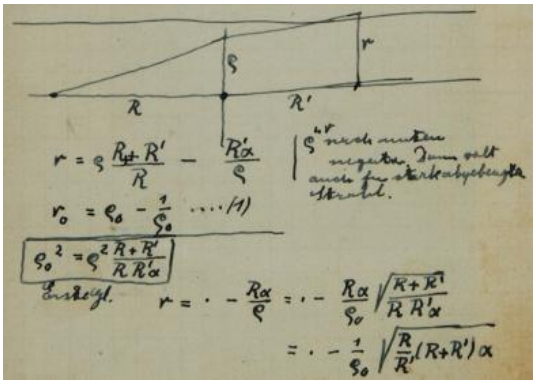

**Figure 1**: Published as part of the Collected Papers of Albert Einstein, Vol. 3, p. 585; Reprinted by permission of Princeton University Press

In one of his notebooks, presumably during a visit to Berlin in April 1912, Einstein recorded the fundamental characteristics of a gravitational lens (fig.1). This notebook contains sketches of the basic concepts and formulae to describe the gravitational lens. However, because other terrestrial astronomers at the time, including Einstein, felt that the observational possibilities of the phenomenon were too low, he did not publish the study until 1936 at the request of an amateur engineer by the name of Rudi W. Mandl.

At the urging of this amateur scientist, we finally saw the beginnings of this study on gravitational lensing. As we mentioned in the introduction part, gravitational lensing is a phenomenon where the gravity of a massive object, like a galaxy, a cluster of galaxies or black hole, bends the path of light from a more distant object (shown in fig.2). This bending of light causes the distant object to appear distorted, magnified, or multiplied. It's similar to how a glass lens bends light to focus or magnify an image, but in this case, the "lens" is the gravitational field of a massive celestial body.

From the study of Einstein (1936), we could derive the Einstein radius step by step. Assuming that the entire mass $M$ of the lensing object $L$ is centralized at its core, for a point mass the deflection can be described by expression we have derived in the class (Lattimer (2024), page 15):

$$\alpha_1 = \frac{4GM}{bc^2} \tag{1}$$

where $b$ is the impact parameter, $G$ is the gravitational constant, $c$ is the speed of light. Acknowledging that, for small angles with the angle denoted in radians, the closest approach point $b_1$ at an angle $\theta_1$ for the lens $L$,

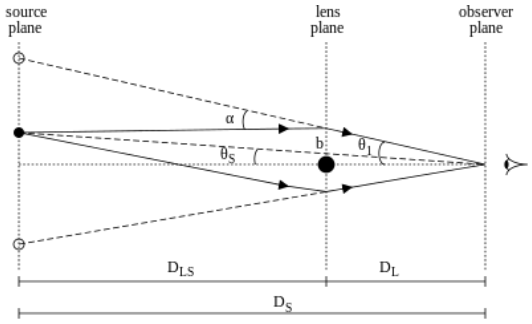


**Figure 2**: Schematic of Gravitational Lens (Credit: Krishnavedala)

located at a distance $D_L$, is determined by $b_1 = \theta_1 D_L$, we can reformulate the bending angle $\alpha_1$ as follows:

$$\alpha_1(\theta_1) = \frac{4G}{c^2}\frac{M}{\theta_1}\frac{1}{D_L} \tag{2}$$

Based on the fig.2, $\theta_S$ is the angle we could see the source without lens, $\theta_1$ is the angle we observed source with lens. From the figure, we could find that the vertical distance of the angle $\theta_1$ at a distance $D_s$ is the same as the sum of the two vertical distances $\theta_S D_S$ and $\alpha_1 D_{LS}$(where $D_{LS}$ is the horizontal distance between source and lens), then we have the lens equation:

$$\theta_1 D_S = \theta_S D_S + \alpha_1 D_{LS} \tag{3}$$

After rearranged, and substitute eq.(2) into it, we have:

$$\frac{4G}{c^2}\frac{M}{\theta_1}\frac{1}{D_L} = \frac{D_S}{D_{LS}}(\theta_1 - \theta_S) \tag{4}$$

Rearranging it again, we have:

$$\theta_1 - \theta_S = \frac{4G}{c^2}\frac{M}{\theta_1}\frac{D_{LS}}{D_S D_L} \tag{5}$$

If the source is right behind the lens, namely $\theta_s = 0$, then lens equation for a point mass gives a characteristic value for $\theta_1$, which is called the Einstein angle (denoted $\theta_E$):

$$\theta_E = \left(\frac{4GM}{c^2}\frac{D_{LS}}{D_S D_L}\right)^{1/2} \tag{6}$$

The Einstein angle, associated with a point mass, offers a practical linear scale for normalizing lensing variables. When expressed through the Einstein angle, the lens equation for a point mass transforms into

$$\theta_1 = \theta_S + \frac{\theta_E^2}{\theta_1} \tag{7}$$

Thus, we have:

$$\theta_E = \left(\frac{M}{10^{11.09} M_\odot}\right)^{1/2} \left(\frac{D_L D_S / D_{LS}}{\text{Gpc}}\right)^{-1/2} \text{ arcsec} \tag{8}$$

For SN Zwicky, the Einstein Radius is about $\theta_E \approx 0.9'' \left(\frac{M}{10^{11.09} M_\odot}\right)^{1/2} \left(\frac{D_L D_S / D_{LS}}{\mathrm{Gpc}}\right)^{-1/2}$ (Goobar et al. (2023)).

## 3. THE QUADRUPOLE GRAVITATIONAL LENS

Based on the study of Turyshev & Toth (2021a), we could followed their steps to derive the quartic equation for the quadrupole gravitational lens. Their approach is based on a previously developed solution (Turyshev & Toth (2021b)) focusing on the propagation of high-frequency electromagnetic (EM) waves. In this framework, we will neglect terms proportional to $(kr)^{-1}$ and consider cases where the distance $r$ from the gravitational lens is much greater than the Schwarzschild radius $r_g$ of the lens. Then We analyze the EM field within the strong interference region of the gravitational lens (see fig.3).

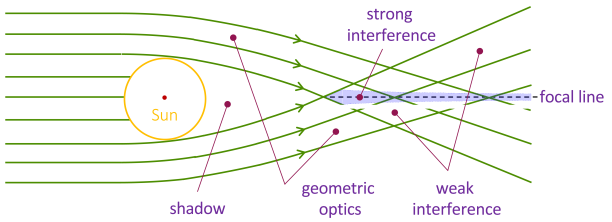


**Figure 3**: The different optical regions of the SGL with respect to light from a source at infinity. (From Turyshev & Toth (2019), fig.2)

For the analysis, we will utilize a coordinate system centered on the lens, with the $z$-axis aligned with the wavevector $\mathbf{k}$ of the incoming wave. We introduce the impact parameter vector $\mathbf{b}$, and define an image plane. This plane, located a distance $z$ from the lens, captures and projects light from the source to form an image. Locations within this image plane are denoted by $\mathbf{x}$. Additionally, we define $\mathbf{s}$ as the unit vector in the direction of the lens's rotation axis:

$$\begin{aligned} \mathbf{b} &= b(\cos\phi_\xi, \sin\phi_\xi, 0) = b\mathbf{n}_\xi \\ \mathbf{x} &= \rho(\cos\phi, \sin\phi, 0) = \rho\mathbf{n} \\ \mathbf{s} &= (\sin\beta_s \cos\phi_s, \sin\beta_s \sin\phi_s, \cos\beta_s) \end{aligned} \tag{9}$$

In this geometry, up to terms of $\mathcal{O}(r_g^2, \rho^2/z^2)$, the EM field in the image plane is in the following form:

$$\begin{pmatrix} E_\rho \\ H_\rho \end{pmatrix} = \begin{pmatrix} H_\phi \\ -E_\phi \end{pmatrix} = E_0 \sqrt{2\pi k r_g} e^{i\sigma_0} B(\mathbf{x}) e^{i(kz-\omega t)} \begin{pmatrix} \cos\phi \\ \sin\phi \end{pmatrix} \tag{10}$$

where $\sigma_0 = -kr_g \ln kr_g/e - \pi/4$ and the quantity $B(\mathbf{x})$ is the complex amplitude of the EM field, which is:

$$\begin{aligned} B(\mathbf{x}) = \frac{1}{2\pi} \int_0^{2\pi} d\phi_\xi \exp\Bigg[ -ik \Bigg( & \sqrt{\frac{2r_g}{r}} \rho \cos(\phi_x i - \phi) \\ & + 2r_g \sum_{n=2}^{\infty} \frac{J_n}{n} \left(\frac{R_\odot}{\sqrt{2r_g r}}\right)^n \sin^n \beta_s \cos[n(\phi_x i - \phi_s)] \Bigg) \Bigg] \end{aligned} \tag{11}$$

where $J_n$ represents the zonal harmonics which characterizing the external gravitational potential of an axisymmetric lens (Turyshev & Toth (2019)). From the study of Turyshev & Toth (2021c), we know that each of the zonal harmonics, $J_n$, produces a distinct set of caustics. Now, we are focusing on the diffraction integral eq.(11) for a quadrupole lens (where only consider $J_2$). To simplify the integral eq.(11), we define two new constants $\alpha$ and $\beta_2$:

$$\alpha = k\sqrt{\frac{2r_g}{r}}, \qquad \beta_2 = kr_g J_2 \left(\frac{R_\odot}{\sqrt{2r_g r}}\right)^2 \sin^2\beta_s \tag{12}$$

And both of them present a clear physics meaning. $\alpha$ stand for the spatial frequency of the characteristic pattern formed due to the quadrupole moment, and $\beta_2$ is the phase shift accumulated by the EM wave due to $J_2$. (see the details in Turyshev & Toth (2021c)) Now, the diffraction integral eq.(11) is in the form:

$$\begin{aligned} B(\mathbf{x}) = \frac{1}{2\pi} \int_0^{2\pi} d\phi_\xi \exp\big[ -i(\alpha\rho\cos(\phi_x - \phi) \\ + \beta_2 \cos[2(\phi_\xi - \phi_s)]) \big] \end{aligned} \tag{13}$$

Now, we will consider the integral eq.(13) and recognize that its oscillatory behavior is driven by the phase $\varphi$ which is in the form:

$$\varphi(\rho, \phi) = -(\alpha\rho\cos(\phi_\xi - \phi)) + \beta_2 \cos[2(\phi_\xi - \phi_s)]) \tag{14}$$

Based on the method of stationary phase, we need to derivative $\varphi$ up to second-order, then we have:

$$\varphi' = \frac{d\varphi}{d\phi_\xi} = \alpha\rho\sin(\phi_\xi - \phi) + 2\beta_2 \sin[2(\phi_\xi - \phi_s)] \tag{15}$$

$$\varphi'' = \frac{d^2\varphi}{d\phi_\xi^2} = \alpha\rho\cos(\phi_\xi - \phi) + 4\beta_2 \cos[2(\phi_\xi - \phi_s)] \tag{16}$$

The phase will be stationary if its first derivative eq.(15) vanishes. Through setting $\varphi' = 0$, we have:

$$\alpha\rho\sin(\phi_\xi - \phi) + 2\beta_2 \sin[2(\phi_\xi - \phi_s)] = 0 \tag{17}$$

Define that $\mu = 2(\phi - \phi_s)$, then we have:

$$\begin{aligned} \alpha\rho\sin(\phi_\xi - \phi) + 2\beta_2(1 - 2\sin^2(\phi_\xi - \phi))\sin\mu \\ + 4\beta\sin(\phi_\xi - \phi)\cos(\phi_\xi - \phi)\cos\mu = 0 \end{aligned} \tag{18}$$

Change the variables by x, which satisfies:

$$\sin(\phi_\xi - \phi) = x, \quad \cos(\phi_\xi - \phi) = \pm\sqrt{1-x^2} \tag{19}$$

Then, eq.(18) is transformed to:

$$\alpha\rho x + 2\beta_2 \sin\mu(1-2x^2) \pm 4\beta_2 \cos\mu x\sqrt{1-x^2} = 0 \tag{20}$$

After rearranged eq.(20), and squaring both sides, we have:

$$\begin{aligned} 16\beta_2^2 x^4 - 8\alpha\rho\beta_2 \sin\mu x^3 + ((\alpha\rho)^2 - 16\beta_2^2)x^2 \\ +4\alpha\rho\beta_2 \sin\mu x + 4\beta_2^2 \sin^2\mu = 0 \end{aligned} \tag{21}$$

If $\beta_2 = 0$, eq.(21) have the result of $x = 0$ or $\sin(\phi_\xi - \phi) = 0$ leading to $\phi_x i = \phi$. This outcome aligns with the behavior in a monopole gravitational field, where light propagates in a plane (Turyshev & Toth (2021a), Appendix A1). If $\beta_2 \neq 0$, divide eq.(21) by $16\beta_2^2$, and define $\eta = \alpha\rho/4\beta_2$, then we have the main equation for the quadrupole gravitational lens:

$$x^4 - 2\eta\sin\mu x^3 + (\eta^2-1)x^2 + \eta\sin\mu x + \frac{1}{4}\sin^2\mu = 0 \tag{22}$$

Based on eq.(9), eq.(19) can be expressed in a way that highlights their geometric nature, specifically, $\cos(\phi_\xi - \phi) = (\mathbf{n}_\xi \cdot \mathbf{n})$ and $\sin(\phi_\xi - \phi) = |[\mathbf{n} \times [\mathbf{n}_\xi \times \mathbf{n}]]|$, which precisely represent the Cartesian projections of the observer's position vector with respect to the impact parameter vector. Consequently, for any given observer's position, $\rho\mathbf{n}$, there exists a corresponding $b\mathbf{n}_\xi$ such that the quantities in eq.(9) will span all values $x \in [-1, 1]$.

Followed by the rules we introduced in the appendix A (eq.(A3-A6)), we have

$$\begin{aligned} x_{1,2}(\eta,\mu) =& \frac{1}{2}\eta\sin\mu - S \pm \big(-4S^2 - 2(\eta^2-1) \\ &+ 3\eta^2\sin^2\mu + \frac{\eta^3\cos^2\mu\sin\mu}{S}\big)^{1/2} \\ x_{3,4}(\eta,\mu) =& \frac{1}{2}\eta\sin\mu + S \pm \big(-4S^2 - 2(\eta^2-1) \\ &+ 3\eta^2\sin^2\mu - \frac{\eta^3\cos^2\mu\sin\mu}{S}\big)^{1/2} \end{aligned} \tag{23}$$

Where the quantities $S$ and $Q$ are:

$$\begin{aligned} S =& \frac{1}{2}\left\{-\frac{2}{3}(\eta^2-1) + \eta^2\sin^2\mu \right. \\ &\left. + \frac{1}{3}\left(Q + \frac{(\eta^2-1)^2 + 3(2\eta^2+1)\sin^2\mu}{Q}\right)\right\}^{1/2} \end{aligned} \tag{24}$$

$$\begin{aligned} Q =& \{(\eta^2-1)^3 + 9(\eta^2-1)^2\sin^2\mu + \frac{27}{2}\eta^2\sin^2\mu(1+\sin^2\mu) \\ &+ \cos^2\mu[(27(\eta^2-1)^3 + (\frac{27}{2})^2\eta^4\sin^2\mu)\sin^2\mu]^{1/2}\}^{1/3} \end{aligned} \tag{25}$$

Here, the discriminant is:

$$\Delta(\eta,\mu) = -((\eta^2-1)^3 + \frac{27}{4}\eta^4\sin^2\mu)\sin^2\mu \tag{26}$$

Before we evaluate the integral eq.(13), we have to

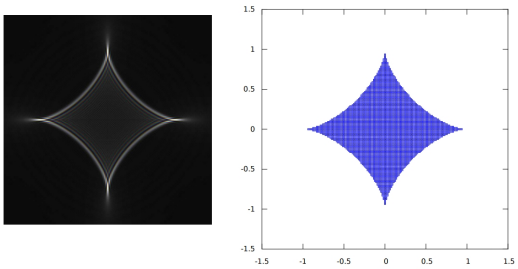

**Figure 4**: Left: A typical astroid caustic;Right: the region in the image plane, where the quartic discriminant $\Delta$ (eq.(26)) is positive. (Turyshev & Toth (2021a), fig.2)

resolve the ambiguity of $\sin(\phi_\xi - \phi) = \sin(\pi - (\phi_\xi - \phi))$. Turyshev & Toth (2021a) introduced an alternate form of the quartic equation, written in terms of $y = \sqrt{1-x^2} = \cos(\phi_\xi - \phi)$:

$$y^4 + 2\eta\cos\mu y^3 + (\eta^2-1)y^2 - 2\eta\cos\mu y + \frac{1}{4}\sin^2\mu - \eta^2 = 0 \tag{27}$$

Based on this approach, we are able to identify all the pairs of the solutions of the quartic equation eq.(22) (which is shown on Appendix B). With those results to evaluate the integral eq.(13).

Having determined both $\sin(\phi_\xi - \phi)$ and $\cos(\phi_\xi - \phi)$, we are now equipped to depict the quantity $(\phi_\xi - \phi)$ on the image plane, which is characterized by $\eta = \left(\frac{\alpha}{4\beta^2}\right)\rho$ as the dimensionless radial coordinate, and $\phi$ as the angular coordinate. The resulting visualization, presented in fig.8 (left), provides valuable insights. It reveals that the central region of the three-dimensional structure, delineated by the four roots, exhibits considerable complexity. To gain a clearer understanding of this region, we can also examine it from a point perpendicular to the image plane, as illustrated in Fig.8 (right). The cross-sectional shape of this region mirrors the astroid typical of the quadrupole gravitational lens.

Based on the numerical analysis above, we could imagine point sources with a quadrupole lens. Fig.5 display the model with different position of the quadrupole lens.

By comparing the observations (fig.6) to the simulations (fig.5), the image from this simulation closely approximates the observed image of SN Zwicky.

## 4. SN ZWICKY

The study of SN Zwicky, a rare supernova event of significant interest, opens new method for understanding

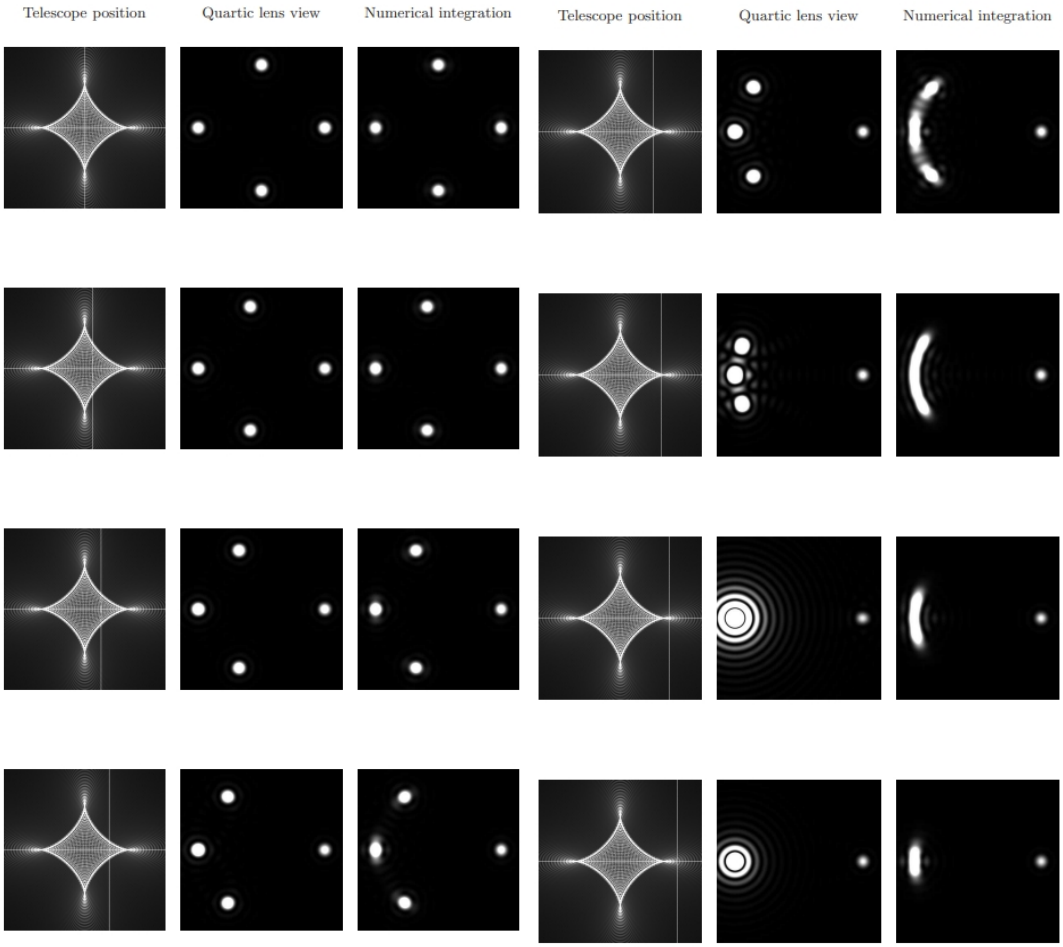


**Figure 5**: The first column shows the telescope position (thin vertical gray line) overlayed the cross-sectional view of the quartic solution, with $\eta$ on the horizontal axis and $(\phi_\xi - \phi)$, given in degrees, on the vertical. Second column: Crosshairs indicating the same telescope location with respect to the PSF. Third column: the view through the telescope, modeled using the quartic solution. Fourth column: Telescopic view via numerical integration.(Turyshev & Toth (2021a), fig.7-8)

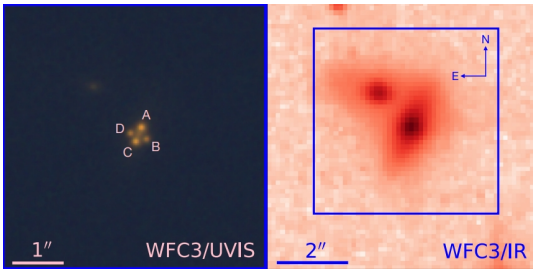


**Figure 6**: (left) A WFC3/UVIS combined color image (R=F814W, G=F625W, B=F475W) of SN Zwicky, with the multiple images labeled as A-D. (Right) WFC3/IR F160W image of the galaxy lensing of SN Zwicky, where the multiple images are not resolved.(Goobar et al. (2022), fig.3)

the universe's mysteries, including the nature of dark matter, the cosmic distance scale, and the evolution of supernovae. While our paper primarily focuses on the mathematical descriptions of gravitational lensing by a quadrupole gravitational lens, here we introduce the application to these phenomena, particularly in relation to SN Zwicky.

### 4.1. *Dark Matter and Distance Scale*

The gravitational lensing effects observed around SN Zwicky provide a unique opportunity to probe the distribution and properties of dark matter. Magnified by a strong gravitational lensing, the characteristics of SN Zwicky is presented much better than any other normal distant supernova. Given the known redshifts of both the lensing galaxy and the background source, the lensing configuration depicted in Hubble Space Telescope imagery (fig.(7)) allows for the determination of the total mass within the Einstein radius, regardless of the luminosity of the material. This mass estimation, when

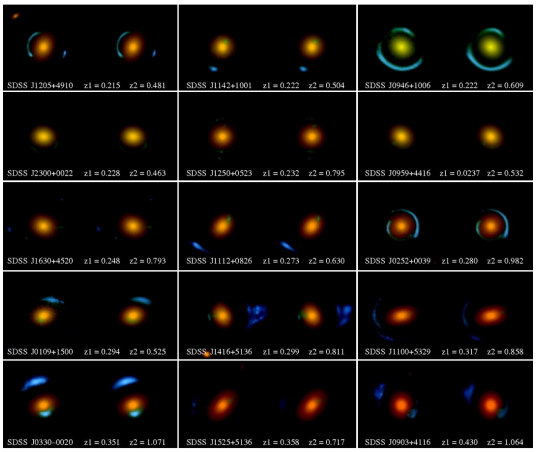


**Figure 7**: Hubble Space Telescope images of a selection of elliptical lenses from the SLACS survey (Bolton et al. (2008))

combined with measurements derived from the velocity dispersion of stars within the lensing galaxy, enables the calculation of the mass density profile, $\rho(r)$, as a function of distance from the galactic center (Ellis (2010)). Notably, this mass distribution extends beyond the spatial confines of the observable baryonic matter, providing unequivocal evidence for the presence of dark matter.

Furthermore, SN Zwicky's lensing effects contribute to our understanding of the cosmic distance scale. The magnification and distortion of light, as described by our wave-optical study, allow for more precise measurements of distances in the universe. By comparing the observed brightness of SN Zwicky with its intrinsic luminosity, inferred through lensing models, we can refine our estimates of its distance from Earth, thereby enhancing the accuracy of the cosmic distance ladder.

### 4.2. *Time Delays and Matter Distribution*

Due the advantages of SNe (Fade quickly, predictable light curves, weak impact of microlensing), the time delays observed in the light curves of lensed images of SN Zwicky are invaluable for probing the matter distribution in the universe. The time delay between images of a supernova, as seen through gravitational lensing, varies significantly based on the differences in geometry and gravitational potential along each path. For lenses on the scale of galaxies, these delays can range from hours to months, while for lenses the size of galaxy clusters, the delays can extend to years. It can be meticulously analyzed to reveal the mass distribution of the intervening lensing object. This analysis not only aids in understanding the lens's structure but also provides insights into the larger-scale matter distribution, including both luminous and dark matter components. However, based on the research of Pierel et al. (2023), the small time delays of SN Zwicky (which is explained by the relatively small Einstein radius) leads that it is not a good sample to measure $H_0$.

### 4.3. *Supernova Evolution*

The study of SN Zwicky through gravitational lensing offers a unique perspective on the evolution of supernovae. Based on the magnifying effect ($\mu \approx 25$, Pierel et al. (2023)) of lenses, we can observe more distant supernovae more clearly. The higher time-resolved observations made possible by lensing phenomena allow astronomers to dissect the light curves of supernovae in unprecedented detail. This clarity enables the identification of subtle features in the supernova's evolution, shedding light on the mechanisms driving these cataclysmic events.

## 5. CONCLUSION

In this study, baesd on the study of Turyshev & Toth (2021a), we have re-derived a comprehensive wave-optical analysis of the Einstein cross phenomenon as manifested through the influence of a quadrupole gravitational lens followed steps by Turyshev & Toth (2021a). This investigation has elucidated the intricate interplay between wave optics and gravitational lensing, revealing how the quadrupole moment of a gravitational lens shapes the observed light patterns into the characteristic Einstein cross configuration.

Through rigorous mathematical modeling, we derived expressions and solutions for the electromagnetic field in the vicinity of a quadrupole gravitational lens, taking into account the complex geometrical and physical interactions at play. This research help us demonstrate and have a deeper comprehension of that the spatial frequency and phase differences induced by the lens lead to the formation of an Einstein cross with distinct features, dependent on the lens's quadrupole moment and the observer's position, and the applications of strong gravitational lensed SNe.

However, this study is not without limitations. Limited by my low computer skills, I was unable to programmatically reproduce the simulation results of the study. It would be interesting to have the results from SN Zwicky fitted by a numerical solution and plotted against the above model for comparison in the next report.

In conclusion, the wave-optical study of the Einstein cross formed by a quadrupole gravitational lens contributes valuable insights into the field of gravitational lensing and wave optics. By advancing our understanding of how light interacts with gravitational fields, this

work paves the way for future explorations into the cosmos, offering glimpses into the distant universe.

## APPENDIX

### A. QUARTIC EQUATION

The four roots of the general quartic equation in the form of:

$$ax^4 + bx^3 + cx^2 + dx + e = 0 \tag{A1}$$

with $a \neq 0$, have the following form:

$$x_{1,2} = -\frac{b}{4a} - S \pm \frac{1}{2}\sqrt{-4S^2 - 2P + \frac{q}{S}} \tag{A2}$$

$$x_{3,4} = -\frac{b}{4a} + S \pm \frac{1}{2}\sqrt{-4S^2 - 2P - \frac{q}{S}} \tag{A3}$$

where $p$ and $q$ are given as

$$p = \frac{8ac - 3b^2}{8a^2}, \qquad q = \frac{b^3 - 4abc + 8a^2d}{8a^3} \tag{A4}$$

and $S$ and $Q$ have the form

$$S = \frac{1}{2}\left[-\frac{2}{3}p + \frac{1}{3a}\left(Q + \frac{\Delta_0}{Q}\right)\right]^{1/2}, \qquad Q = \left[\frac{1}{2}\left(\Delta_1 + \sqrt{\Delta_1^2 - 4\Delta_0^3}\right)\right]^{1/3} \tag{A5}$$

where $\Delta_0$ and $\Delta_1$ are

$$\Delta_0 = c^2 - 3bd + 12ae, \qquad \Delta_1 = 2c^3 - 9bcd + 27b^2e + 27ad^2 - 72ace \tag{A6}$$

The quantity

$$\Delta = -\frac{1}{27}(\Delta_1^2 - 4\Delta_0^3) \tag{A7}$$

is recognized as the discriminant of the quartic equation. When $\Delta > 0$ either all four roots of the quartic equation are real orall four roots are complex; When $\Delta \leq 0$, there will be typically two real roots.

### B. PAIRS OF THE SOLUTIONS

$$\begin{aligned}
& \sin(\phi_\xi - \phi) = x_1(\eta, \mu) \\
\mu \in ]0, \frac{1}{2}\pi[: \quad & \cos(\phi_\xi - \phi) = \sqrt{1 - x_1^2}, \\
\mu \in ]\frac{1}{2}\pi, \pi[: \quad & \cos(\phi_\xi - \phi) = -\sqrt{1 - x_1^2}, \\
\mu \in ]\pi, \frac{3}{2}\pi[: \quad & \cos(\phi_\xi - \phi) = \sqrt{1 - x_1^2}, \\
\mu \in ]\frac{3}{2}\pi, 2\pi[: \quad & \cos(\phi_\xi - \phi) = -\sqrt{1 - x_1^2}
\end{aligned} \tag{B8}$$

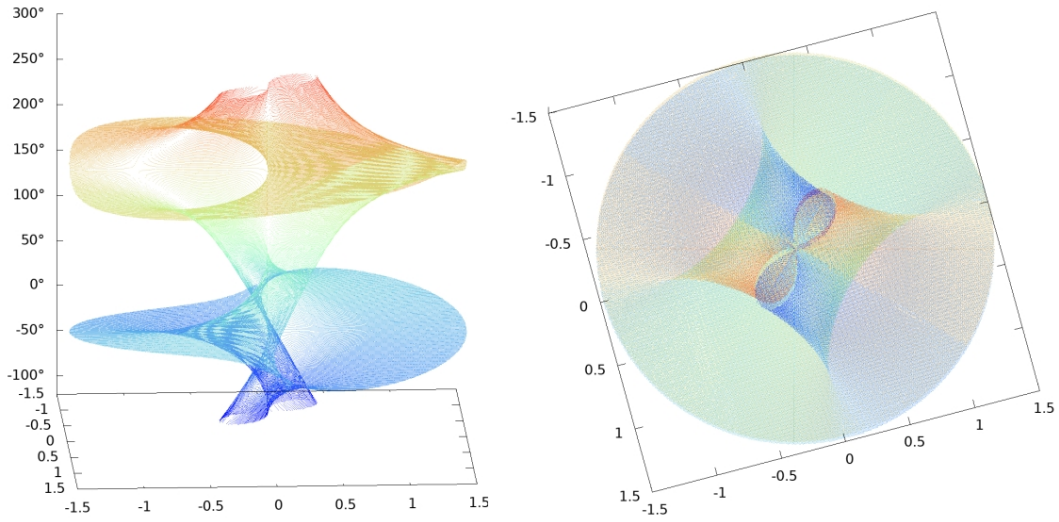


**Figure 8**: Plot of solution space.(Turyshev & Toth (2021a), fig.3)

$$
\begin{aligned}
& & \sin(\phi_\xi - \phi) &= x_2(\eta,\mu) \\
\mu \in ]0, \frac{1}{2}\pi[: & & \cos(\phi_\xi - \phi) &= -\sqrt{1-x_2^2}, \\
\mu \in ]\frac{1}{2}\pi, \pi[: & & \cos(\phi_\xi - \phi) &= \sqrt{1-x_2^2}, \\
\mu \in ]\pi, \frac{3}{2}\pi[ \wedge \frac{1}{4}\sin^2\mu - \eta^2 \geq 0: & & \cos(\phi_\xi - \phi) &= -\sqrt{1-x_2^2}, \\
\mu \in ]\pi, \frac{3}{2}\pi[ \wedge \frac{1}{4}\sin^2\mu - \eta^2 < 0: & & \cos(\phi_\xi - \phi) &= \sqrt{1-x_2^2}, \\
\mu \in ]\frac{3}{2}\pi, 2\pi[ \wedge \frac{1}{4}\sin^2\mu - \eta^2 \geq 0: & & \cos(\phi_\xi - \phi) &= \sqrt{1-x_2^2} \\
\mu \in ]\frac{3}{2}\pi, 2\pi[ \wedge \frac{1}{4}\sin^2\mu - \eta^2 < 0: & & \cos(\phi_\xi - \phi) &= -\sqrt{1-x_2^2}
\end{aligned}
\tag{B9}
$$

$$
\begin{aligned}
& & \sin(\phi_\xi - \phi) &= x_3(\eta,\mu) \\
\mu \in ]0, \frac{1}{2}\pi[ \wedge \frac{1}{4}\sin^2\mu - \eta^2 \geq 0: & & \cos(\phi_\xi - \phi) &= \sqrt{1-x_3^2}, \\
\mu \in ]0, \frac{1}{2}\pi[ \wedge \frac{1}{4}\sin^2\mu - \eta^2 < 0: & & \cos(\phi_\xi - \phi) &= -\sqrt{1-x_3^2}, \\
\mu \in ]\frac{1}{2}\pi, \pi[ \wedge \frac{1}{4}\sin^2\mu - \eta^2 \geq 0: & & \cos(\phi_\xi - \phi) &= -\sqrt{1-x_3^2}, \\
\mu \in ]\frac{1}{2}\pi, \pi[ \wedge \frac{1}{4}\sin^2\mu - \eta^2 < 0: & & \cos(\phi_\xi - \phi) &= \sqrt{1-x_3^2}, \\
\mu \in ]\pi, \frac{3}{2}\pi[: & & \cos(\phi_\xi - \phi) &= \sqrt{1-x_3^2}, \\
\mu \in ]\frac{3}{2}\pi, 2\pi[: & & \cos(\phi_\xi - \phi) &= -\sqrt{1-x_3^2}
\end{aligned}
\tag{B10}
$$

$$
\begin{aligned}
& & \sin(\phi_\xi - \phi) &= x_4(\eta, \mu) \\
\mu \in ]0, \frac{1}{2}\pi[: & & \cos(\phi_\xi - \phi) &= -\sqrt{1 - x_4^2}, \\
\mu \in ]\frac{1}{2}\pi, \pi[: & & \cos(\phi_\xi - \phi) &= \sqrt{1 - x_4^2}, \\
\mu \in ]\pi, \frac{3}{2}\pi[: & & \cos(\phi_\xi - \phi) &= -\sqrt{1 - x_4^2}, \\
\mu \in ]\frac{3}{2}\pi, 2\pi[: & & \cos(\phi_\xi - \phi) &= \sqrt{1 - x_4^2}
\end{aligned}
\tag{B11}
$$

## REFERENCES


Bolton, A. S., Burles, S., Koopmans, L. V. E., et al. 2008, The Astrophysical Journal, 682, 964, doi: 10.1086/589327

Einstein, A. 1936, Science, 84, 506, doi: 10.1126/science.84.2188.506

Ellis, R. S. 2010, Philosophical Transactions of the Royal Society A: Mathematical, Physical and Engineering Sciences, 368, 967, doi: 10.1098/rsta.2009.0209

Goobar, A., Johansson, J., Schulze, S., et al. 2023, Nature Astronomy, 7, 1098–1107, doi: 10.1038/s41550-023-01981-3

Goobar, A. A., Johansson, J., Dhawan, S., et al. 2022, Transient Name Server AstroNote, 180, 1

Lattimer, J. 2024, AST 390 Orbits in General Relativity, https://www.astro.sunysb.edu/lattimer/AST390/gr_orbit.pdf/

Pierel, J. D. R., Arendse, N., Ertl, S., et al. 2023, ApJ, 948, 115, doi: 10.3847/1538-4357/acc7a6

Sauer, T. 2010, A brief history of gravitational lensing, https://www.einstein-online.info/en/spotlight/grav_lensing_history/

Turyshev, S. G., & Toth, V. T. 2019, Physical Review D, 100, doi: 10.1103/physrevd.100.084018

—. 2021a, Phys. Rev. D, 104, 124033, doi: 10.1103/PhysRevD.104.124033

—. 2021b, Physical Review D, 103, doi: 10.1103/physrevd.103.064076

—. 2021c, Physical Review D, 104, doi: 10.1103/physrevd.104.024019